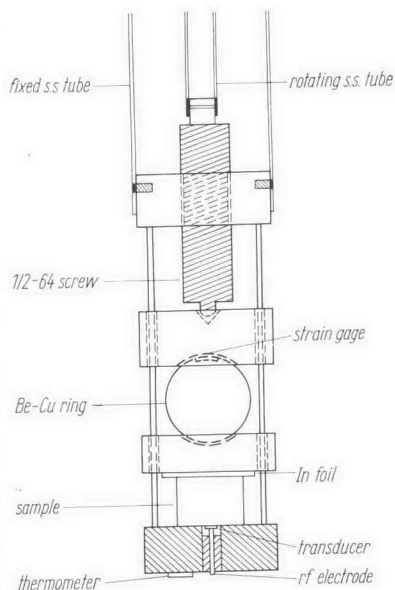


Fig. 2. The sample holder and stress apparatus



The data were taken with the sample located in a cold finger immersed in a pumped-helium bath, and the sample temperatures were in the range 1.2 to 1.5 °K.

A schematic drawing of the apparatus used to apply the stress is shown in Fig. 2. A beryllium-copper ring was used to take up most of the displacement imparted by the screw and to measure the stress by means of a strain gage mounted on the ring. The load on the sample was determined with an estimated uncertainty of 3%. The maximum stresses used were about 8×10^7 dyn/cm².

The experimental data were obtained by the phase shift method. This method exploits the fact that when an extremal Fermi surface area, which produces a set of quantum oscillations, undergoes a small change, a shift of the period results and may thus lead to a measureable change in the field at which an extremum of the oscillations occurs. The change in the extremal area, A , produced by the stress, σ , can be related to the change in the phase, φ , of the oscillations by the equation [12]

$$\frac{d \ln A}{d\sigma} = H \left(\Delta \frac{1}{H} \right) \frac{d\varphi}{d\sigma}, \quad (1)$$

where H is the average field for the oscillations and $\Delta \frac{1}{H}$ is the period (in inverse Gauss) of the extremal area.

3. Theoretical Calculations

The areas for the orbits studied experimentally were calculated using the Stark-Falicov pseudopotential [8]. The computations were done first for the unstrained condition; the effect of strain was then introduced for comparison with the experimental results.

The calculations under strain were done at one fixed value of stress (6×10^7 dyn/cm² for the needles, and 4×10^7 dyn/cm² for the other orbits), and the lattice strains were determined from the measured low temperature elastic constants of Zn [13, 14]. The strains entered into the calculations in several ways:

A) Both the kinetic energy term and the non-local pseudopotential term depend explicitly on the lengths and relative orientations of various vectors in reciprocal space. These terms are readily calculated in terms of the strained reciprocal lattice vectors. Furthermore, the non-local component is normalized within the unit cell of the crystal, and the volume change under stress must be included.

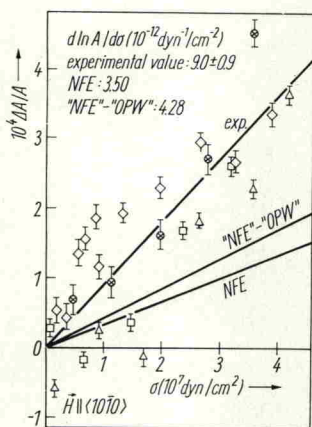


Fig. 3. Experimental points for the lens orbit ζ . Each point corresponds to one sweep of the magnetic field at the stress indicated; the values of $\Delta A/A$ are obtained from the phase shift of the resulting trace with respect to the trace at zero stress. Also shown are the slopes calculated from the NFE-OPW and NFE models

B) Stark and Falicov list the local component values of the pseudopotential for the four smallest reciprocal lattice vectors with non-vanishing structure factors; namely, $\langle 0002 \rangle$, $\langle 10\bar{1}0 \rangle$, $\langle 10\bar{1}1 \rangle$, and $\langle 10\bar{1}2 \rangle$. The change in length of these vectors, due to strain, was taken into account by fitting a polynomial in reciprocal space dimensions to the four tabulated pseudopotential values, and using this polynomial to find the local component in the strained case.

C) One assumption made in the present work is that, even though the Fermi energy obtained by Stark and Falicov from their fitting procedure (0.8005 ryd) differs from the NFE value (0.7076 ryd), the volume dependence is that of the NFE model, i.e., $v^{-2/3}$, where v is the volume of the unit cell.

4. Results and Discussion

The analysis of the experimental data is based on the linear relation between the reciprocals of the magnetic fields for the attenuation peaks and the integers. At sufficiently high fields the phase shift due to a given stress is obtained directly from the spacing of these straight lines caused by the application of the stress. The analysis was carried out on a computer, using a least-squares fit of the inverse field values at the peaks against the integers, and determining the shift of the resulting straight lines with applied stress. The experimental data and

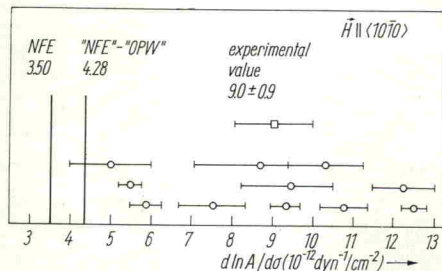


Fig. 4

Fig. 4. Experimental and theoretical results for the lens orbit ζ . Each circle represents the slope obtained for each value of stress used, for each run; the final weighted average is also shown (square), along with the calculated values based on the models discussed in the text (vertical lines)

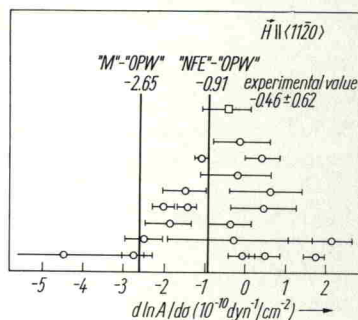


Fig. 5

Fig. 5. Same as Fig. 4, for the β orbit (horizontal arms) with H along $\langle 11\bar{2}0 \rangle$